Hindawi
Mathematical Problems in Engineering
Volume 2022, Article ID 7393586, 12 pages
https://doi.org/10.1155/2022/7393586

Research Article

Influence of Pier Size on its Failure Mode under Near-Fault Vertical Earthquake

Houzheng Xia, Wenjun An, and Lin Zhou

School of Civil Engineering, Jiangxi University of Engineering, Xinyu 330046, China

Correspondence should be addressed to Wenjun An; wjan_ncu@163.com

Received 6 July 2022; Revised 12 August 2022; Accepted 14 September 2022; Published 4 October 2022

Academic Editor: Ji Wang

To calculate the influence of pier size on the pier failure mode, a double-span continuous girder bridge model was selected for analysis. The transient wave function expansion method was used to calculate the excitation conditions required for pier separation and the limit solution of pier longitudinal deformation under pier separation, and the indirect mode superposition method was used to calculate the vertical impact force of the pier-beam. The calculation results show that the higher the pier height, the smaller the section size, the larger the vertical seismic acceleration required to separate the pier-beam, the smaller the vertical contact force of the pier-beam, and the larger the most unfavorable value of the longitudinal deformation of the pier caused by separation. The stress of the bridge pier before and after separation is compared and the influence of separation on the failure of the bridge pier is put forward. The study shows that when pier and beam separation occurs, there may be multiple failure modes superimposed on the pier, and the first failure mode will have variation with the change in pier size.

1. Introduction

The influence of horizontal earthquakes on bridge structures has been studied at home and abroad, and many guiding design suggestions have been given. However, the effect of vertical earthquake is often ignored in bridge design. This is because many monitoring data, especially far-field data, show that horizontal seismic acceleration is usually much greater than vertical seismic acceleration. At the same time, the bridge design mainly considers the vertical load of the structure, and the safety margin and load coefficient are considered in the code to ensure the vertical bearing capacity of the structure. Therefore, it is generally believed that the vertical direction of the structure is safe, and the effect of relatively small vertical seismic excitation on the structure does not need to be considered.

However, with the progress of seismic monitoring levels and the increase in monitoring sites, more and more near-fault monitoring data show that the vertical seismic acceleration is far beyond expectations. A series of studies have been carried out at home and abroad on the impact of vertical earthquakes on structures. Sunil et al. [1] compared unidirectional and bidirectional excitation and found that vertical ground motion had little influence on horizontal response parameters such as displacement and displacement ductility. Still, the higher the damage state was, the more significant the impact was. Shao et al. [2] established the vulnerable earthquake surface under the joint action of horizontal ground motion and VGM by simulating a simply supported bridge model. On this basis, the difference between the damage probability affected by VGM and that not affected by VGM was analyzed, and the sensitive intervals of different damage states were determined. The mechanism of brittleness change of bridge pier under earthquake damage is discussed, and it is pointed out that the difference in seismic demand caused by earthquake damage is the main reason.

However, the vertical excitation value used in the above study is the expected value. In contrast, the near-fault vertical seismic data cannot be simply processed as 2/3 of the horizontal seismic data [3–9]. Near-fault earthquakes are closely related to local site conditions, epicenter distance, and response spectrum period. When the near-fault is a short period of seismic excitation, the peak value of V/H exceeds 2/3 of the specification [10–14]. Geng and Tao [11] found that V/H changed

significantly with the seismic excitation period, with a peak of 1.0 within 0.2 s and a minimum of about 0.4 between 0.2 s and 1.0 s. The long period after 2 s stabilizes at about 0.6. Bozorgnia and Niazi [14] believe that the specified 2/3 is conservative for long periods but unsafe for short period seismic excitation. Liu et al. [15] systematically studied the characteristics of vertical ground motion in Wenchuan, reverted the attenuation process of vertical ground motion, and summarized the variations of V/H in different periods and distances.

In China, the plate rubber bearing is adopted, and the main beam is directly placed on the top of the pier [16, 17], which belongs to the "weak" connection. Most of the horizontal force of the superstructure will not be transmitted to the pier, and the structural link is not easy to damage [18, 19]. In addition, when near-fault vertical seismic excitation occurs, the main beam will produce large deformation and may even be separated from the support [20–22]. The vertical separation of piers and beams not only causes a sizeable vertical collision force of main beams and ports but also affects horizontal seismic response and may lead to structural damage. High amplitude vertical seismic excitation dramatically increases the possibility of structural separation. Tanimura et al. [17, 23] believed that the failure of Nielson bridge support was caused by the vertical collision between the main beam and the bridge pier. So, it is significant to consider the influence of vertical separation on structural failure.

Due to the high amplitude excitation of a near-fault vertical earthquakes and the lack of tensile properties of plate rubber bearings, there is a risk of pier beam separation. The separation will increase the vertical contact force and change the longitudinal dynamic response of the bridge. For the impact force of the pier-beam, Yang and Yin [24] theoretically calculated the change of impact force of the pier-beam under different excitation conditions and structural parameters. Chen et al. [25] calculated the influence of pier and beam separation under different excitation conditions on the bending failure of the pier.

However, the study has the following shortcomings: (1) Only the influence of pier separation on the bending failure of the pier is calculated, and other possible losses are ignored. (2) The longitudinal deformation response only considers the deformation caused by longitudinal excitation and ignores the effect of eccentric vertical compression on the longitudinal deformation of the pier. To analyze the influence of pier height on the dynamic response of bridges, this paper focuses on the following points: (1) Effect of pier size on structure separation. (2) For different pier heights, the change of pier failure modes under pier and beam separation conditions. In this study, the dynamic response of bridge separation with varying sizes of pier is calculated and the influence of separation conditions on the pier failure is studied.

2. The Structural Model

When the bridge is separated vertically, the separation-collision process will increase the vertical contact force of the pier-beam and the change in the longitudinal displacement of the pier. This study focuses on the study of separation characteristics. To simplify the calculation, a double-span continuous beam bridge was selected, with hinge links at both ends of the main beam and rigid links at the bottom of the pier. Springs with different stiffness are used to simulate the axial compression and shear stiffness of bearings. The vertical excitation displacement is $B(t)$, and the longitudinal excitation displacement is $D(t)$. The calculation model is shown in Figure 1.

This study mainly focuses on the conditions under which the vertical seismic excitation in the near field will cause the vertical separation of the pier and beam and the impact of vertical separation on the dynamic response of pier and structural damage. A double span continuous beam bridge is selected as shown in Figure 2. The bridge is a double box prestressed reinforced concrete beam bridge. For double piers, the formula of equivalent structural calculation parameters is given in the code.

Rubber bearing is adopted for the bearing. The bottom of the bearing is rigidly connected with the top of the pier. The main beam is overlapped on the top of the bearing and no tensile connection is set. In addition, in order to simplify the calculation, the change of pier cap and pier area and material is ignored, and it is approximately set as a continuum.

3. Longitudinal Deformation Response of Bridge Pier

The longitudinal displacement response of the bridge consists of three parts, as follows:

$$\begin{aligned} X_1(x,t) &= X_{1s}(x) + X_{1g}(x,t) + X_{1\,d}(x,t), \\ X_2(x,t) &= X_{2s}(x) + X_{2g}(x,t) + X_{2\,d}(x,t), \\ W(\xi,t) &= W_s(\xi) + W_g(\xi,t) + W_d(\xi,t). \end{aligned} \tag{1}$$

Subscripts s, g, and d are static displacement, rigid-body displacement, and dynamic displacement, respectively.

Static displacement of the bridge is as follows:

$$\begin{aligned} X_{1s}(x) &= X_{2s}(x) \\ &= W_s(\xi) \\ &= 0. \end{aligned} \tag{2}$$

Rigid body displacement of the bridge is as follows:

$$\begin{aligned} X_{1g}(x,t) &= X_{2g}(x,t) \\ &= W_g(\xi,t) \\ &= D(t). \end{aligned} \tag{3}$$

Dynamic displacement of the bridge is as follows:

$$\begin{aligned} X_{1\,d}(x,t) &= \sum_{n=1}^{\infty} \varphi_{nb1}(x) q_n(t), \\ X_{2\,d}(x,t) &= \sum_{n=1}^{\infty} \varphi_{nb2}(x) q_n(t), \\ W_d(\xi,t) &= \sum_{n=1}^{\infty} \varphi_{nr}(\xi) q_n(t). \end{aligned} \tag{4}$$

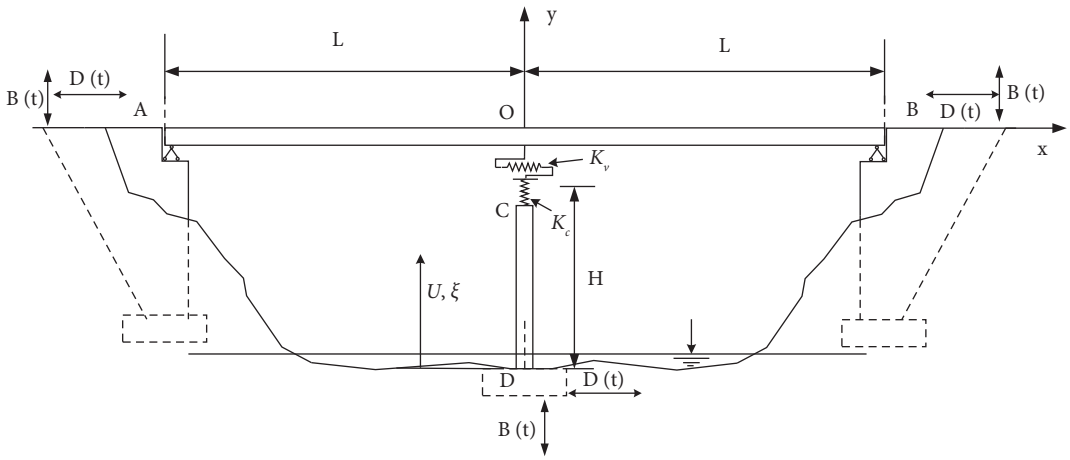

Figure 1: The bridge calculation model.

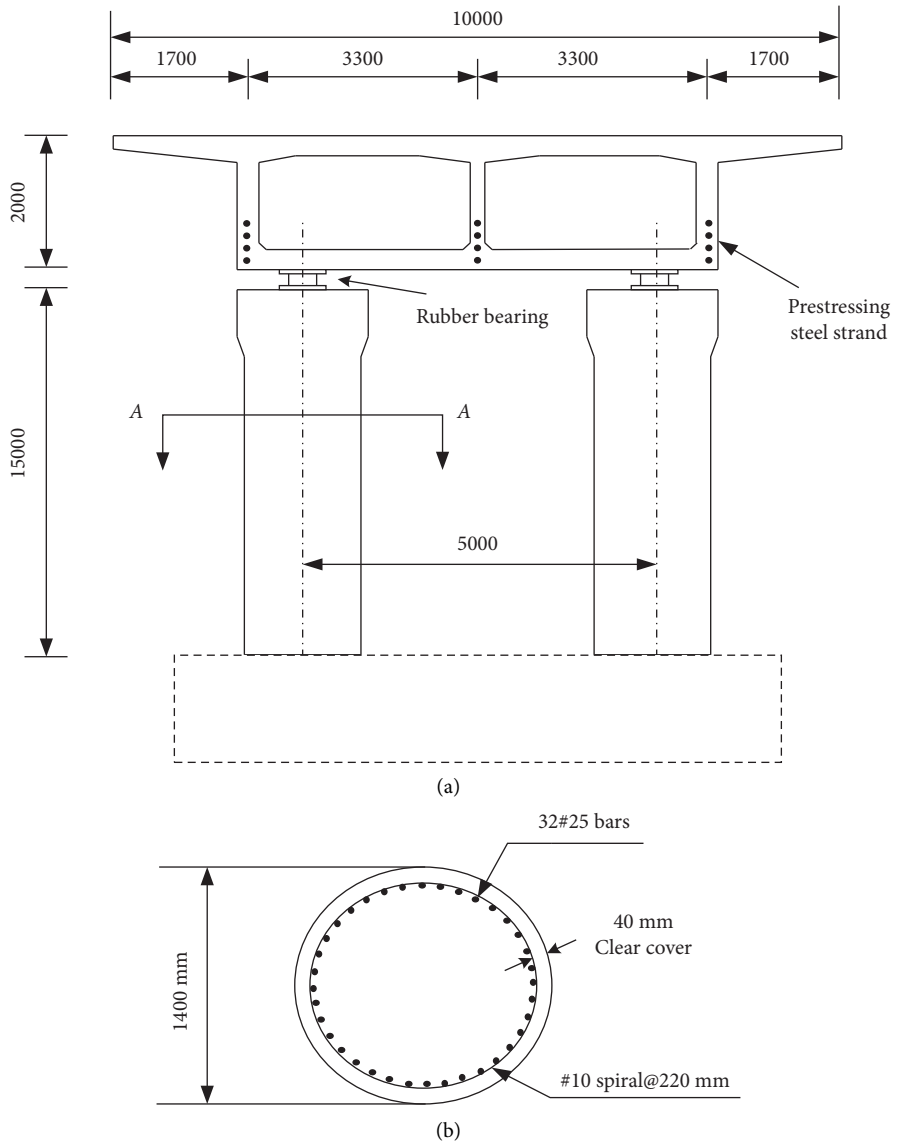

Figure 2: Bridge dimension diagram. (a) Cross-section; (b) pier section.

Dynamic deformation is the multiplication of modal function and time function.

The wave function equations of the bridge can be expressed as follows:

$$\begin{aligned}\varphi_{nb1}(x) &= A_n \sin K_{bn}x + A_n \tan K_{bn}L \cos K_{bn}x,\\ \varphi_{nb2}(x) &= -A_n \sin K_{bn}x + A_n \tan K_{bn}L \cos K_{bn}x,\\ \varphi_{nr}(\xi) &= M_{n1}A_n(\sin K_{rn}\xi - \sinh K_{rn}\xi)\\ &\quad + M_{n2}A_n(\cos K_{rn}\xi - \cosh K_{rn}\xi),\end{aligned} \tag{5}$$

where A_n, M_{n1}, M_{n2} are the coefficients.

From the continuity conditions at the top of the pier and the middle of the main beam, it can be concluded that the longitudinal natural frequency equation of the bridge is as follows:

$$\begin{aligned}&M_{n1}(\sin K_{rn}H - \sinh K_{rn}H) + M_{n2}(\cos K_{rn}H - \cosh K_{rn}H)\\ &= \sin K_{bn}L + \frac{2E_bA_bK_{bn}}{K_V}.\end{aligned} \tag{6}$$

By Laplace transformation, time function $q_n(t)$ can be obtained as follows:

$$\begin{aligned}q_n(t) &= q_n(0)\cos\omega_n t + \frac{\dot{q}_n(0)}{\omega_n}\sin\omega_n t\\ &\quad + \frac{1}{\omega_n}\int_0^t Q_n(\tau)\sin\omega_n(t-\tau)\mathrm{d}\tau.\end{aligned} \tag{7}$$

The calculation method of bridge displacement response in separation stage is the same as that in contact stage. The bridge displacement response in the separation stage is as follows:

$$\begin{aligned}\overline{X}(x,t) &= \overline{X}_s(x) + \overline{X}_g(x,t) + \overline{X}_d(x,t),\\ \overline{W}(\xi,t) &= \overline{W}_s(\xi,t) + \overline{W}_g(\xi,t) + \overline{W}_d(\xi,t).\end{aligned} \tag{8}$$

Static displacement and rigid body displacement in the separation stage of the bridge are as follows:

$$\begin{aligned}\overline{Y}_s(x) &= \overline{U}_s(\xi) = 0,\\ \overline{Y}_g(x,t) &= \overline{U}_g(\xi,t) = D(t).\end{aligned} \tag{9}$$

The wave functions of the bridge structure can be obtained as follows:

$$\begin{aligned}\overline{\varphi}_{nb}(x) &= A_{nb}\sin\overline{k}_{bn}(x+L),\\ \overline{\varphi}_{nr}(\xi) &= A_{nr}((\cosh\overline{K}_{rn}\xi - \cos\overline{K}_{rn}\xi)\\ &\quad + M_{n3}(\sinh\overline{K}_{rn}\xi - \sin\overline{K}_{rn}\xi)),\end{aligned} \tag{10}$$

where A_{nb}, A_{nr}, M_{n2} are the coefficients.

In the separation stage, the dynamic displacement time function is as follows:

$$\begin{aligned}q_{nb}(t^*) &= q_{nb}(t_{2k+1}^+)\cos\omega_{nb}t^* + \frac{\dot{q}_{nb}(t_{2k+1}^-)}{\omega_{nb}}\sin\omega_{nb}t^*\\ &\quad + \frac{1}{\omega_{nb}}\int_{t_{2k+1}^+}^{t^*} Q_{bn}(\tau)\sin\omega_{nb}(t^*-\tau)\mathrm{d}\tau,\\ q_{nr}(t^*) &= q_{nr}(t_{2k+1}^+)\cos\omega_{nr}t^* + \frac{\dot{q}_{nr}(t_{2k+1}^-)}{\omega_{nr}}\sin\omega_{nr}t^*\\ &\quad + \frac{1}{\omega_{nr}}\int_{t_{2k+1}^+}^{t^*} Q_{rn}(\tau)\sin\omega_{nr}(t^*-\tau)\mathrm{d}\tau.\end{aligned} \tag{11}$$

Bridge displacement in collision stage is as follows:

$$\begin{aligned}X(x,t) &= \overline{X}_s(x) + \overline{X}_g(x,t) + \overline{X}_d(x,t) + X_F(x,t),\\ W(\xi,t) &= \overline{W}_s(\xi) + \overline{W}_g(\xi,t) + \overline{W}_d(\xi,t) + W_F(\xi,t).\end{aligned} \tag{12}$$

The static displacements, rigid-body displacements, and dynamic displacements of the main girder and pier are calculated by referring to the separation stage.

In the collision stage, the dynamic response displacement generated by the contact force is as follows:

$$\begin{aligned}X_F(x,t) &= \sum_{n=1}^{\infty}\overline{\varphi}_{nb}(x)\left\{\begin{array}{c} q_{nb}(t_{2k})\cos\omega_{nb}(t-t_{2k}) + \dfrac{\dot{q}_{nb}(t_{2k})}{\omega_{nb}}\sin\omega_{nb}(t-t_{2k})\\ \\ +\displaystyle\int_{t_{2k}}^{t} Q_{nb}\overline{h}_{nb}\mathrm{d}\tau\end{array}\right\},\\ W_F(\xi,t) &= \sum_{n=1}^{\infty}\overline{\varphi}_{nr}(\xi)\left\{\begin{array}{c} q_{nr}(t_{2k})\cos\omega_{nr}(t-t_{2k}) + \dfrac{\dot{q}_{nr}(t_{2k})}{\omega_{nr}}\sin\omega_{nr}(t-t_{2k})\\ \\ +\displaystyle\int_{t_{2k}}^{t} Q_{nb}\overline{h}_{nb}\mathrm{d}\tau\end{array}\right\}.\end{aligned} \tag{13}$$

For detailed calculation of each parameter in the formula, please refer to [25]. The displacement response calculation method of the bridge in the vertical stage are the same as that in the vertical stage.

4. Dynamic Response Calculation of Bridge

4.1. The Separation Characteristics. Under vertical excitation, the dynamic response of the beam bridge is affected by the axial stiffness of the bridge pier. However, among the three parameters of axial stiffness, the elastic modulus of the bridge pier changes a little, and the discussion on the impact of pier beam separation mainly focuses on the two-dimensional parameters of pier height and pier diameter. The pier size coefficient K is introduced, where K is the ratio of pier height to pier diameter, that is, H/D.

Figure 3 shows the bridge separation under different pier sizes when the vertical excitation acceleration is 0.5~1.0 g. To analyze the sensitivity of pier diameter and height to pier-beam separation, only the pier height and pier diameter were changed, respectively, when the pier size coefficient was changed. It can be seen that with the increase of the pier size coefficient, the vertical seismic peak acceleration required for separation also increases. However, the effects of pier height and diameter on pier-beam break are inconsistent. Compared with 'changing the pier diameter', 'changing the pier height' has a more significant impact on the vertical separation of the bridge, because when the pier height changes, the vertical dynamic displacement of the bridge pier changes more.

4.2. Vertical Contact Force of the Pier-Beam. In order to calculate the extreme value of vertical contact force of the pier-beam under different excitation conditions, different excitation accelerations and excitation frequencies are selected for analysis. Figure 4 shows the vertical impact force of the pier-beam under different excitation. The results show that the collision mainly occurs when the excitation frequency is close to the vertical natural frequency of the bridge. The closer the frequency is to the vertical natural frequency, the greater the collision force. This study mainly considers the impact on the pier damage under the vertical separation condition of the pier-beam under the near-field excitation. The selected excitation period is near the first-order natural period of the bridge, and the subsequent analysis takes $T = 0.2$ s.

The bridge is located in an earthquake area of eight degrees and rare occurrence, and the reference peak value of horizontal seismic acceleration is 510 gal. The horizontal design acceleration response spectrum under different periods is referred to the specification [23]. The ratio of vertical seismic acceleration to horizontal acceleration in the near field is 2/3, which may underestimate the vertical seismic effect. For the value of V/H in the follow-up study, please refer to literature [24]. The specific formula is as follows:

$$\lambda = \frac{V}{H} = \begin{cases} \alpha, & T < 0.1, \\ \alpha - \beta(T - 0.1), & 0.1 \le T < 0.3, \\ 0.5, & T \ge 0.3, \end{cases} \quad (14)$$

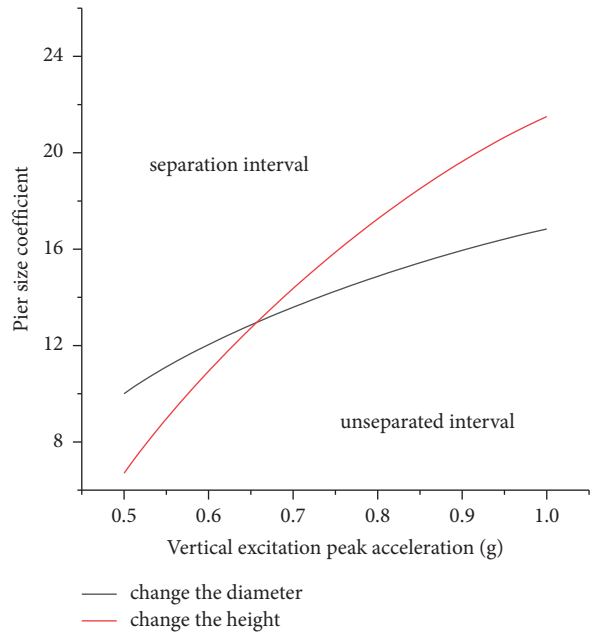

Figure 3: Separation of pier beams with different pier sizes.

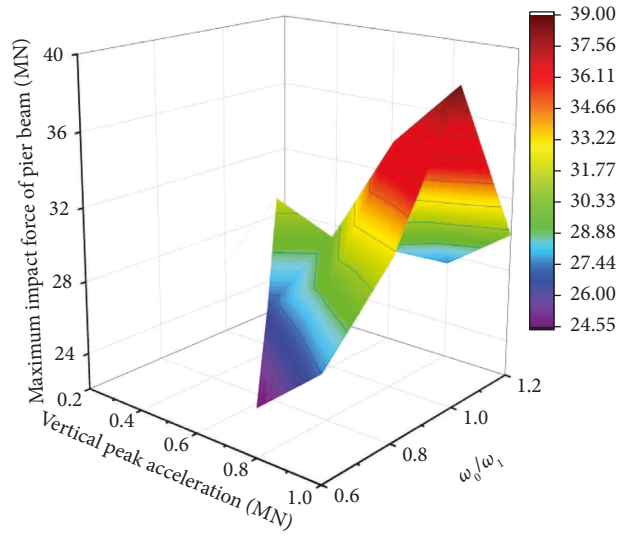

Figure 4: The vertical impact force of the pier-beam.

where T is the vertical seismic period, α is the peak value of V/H, and β is the linear attenuation coefficient. When the epicenter distance is 3 km, 10 km, and 20 km, $\alpha = 1.5$, 1.4, and 1.3, respectively; $\beta = 5$, 4, and 3, respectively.

When the size of the pier is changed, the axial stiffness of the pier changes, affecting the vertical separation of the main beam and the pier. Figure 5 shows the change of vertical contact force of the pier-beam under different pier sizes. With the increase of the pier height and the decrease of the pier cross-sectional area, the vertical contact force between the main beam and the pier gradually decreases until the vertical separation of the structure does not occur. This is because the increase of the pier height and the reduction of the cross-sectional area reduce the axial stiffness of the pier,

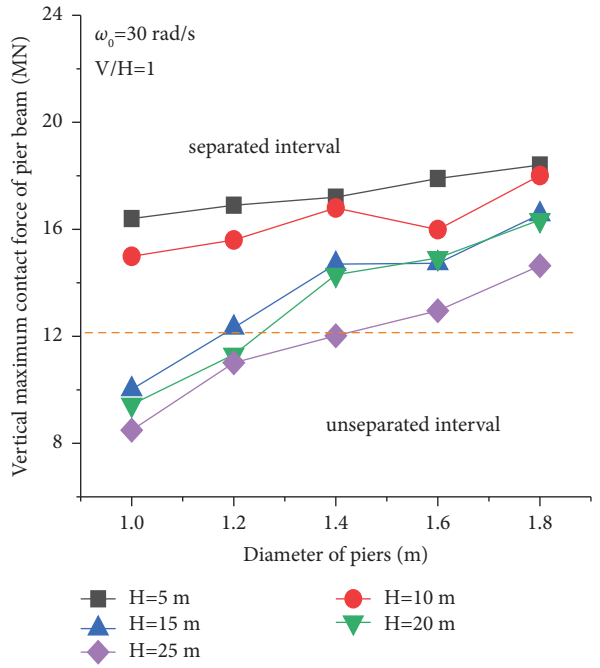

FIGURE 5: Maximum vertical impact force of the pier-beam under different pier sizes.

increase the vertical axial deformation, and reduce the separation probability of the pier-beam.

The impact time of the pier-beam is short, and the forced vibration of the bridge has little influence on the vertical dynamic response of the bridge. When the K value is small, the amplitude of the modal function of the pier wave is large, and the large dynamic displacement of the pier and the dynamic displacement of the main beam is unchanged. As the dynamic deformation trend of the main beam and the pier remains basically the same, the vertical velocity of the middle of the main beam relative to the top of the pier decreases with the decrease of the pier K value at the separation moment. Previous studies indicate that the vertical impact velocity of the girder and pier is determined by the relative speed at the separation moment, and the smaller the impact velocity, the smaller the deformation is.

4.3. Longitudinal Deformation of Bridge Piers. As the coefficient K increases, the generalized force of pier collision increases. As a result, the vertical deformation of pier increases and the vertical impact force decreases when pier and beam collide.

Table 1 shows the ratio of first-order longitudinal natural frequencies of piers at different heights before and after separation. As the height of the pier increases, the rubber bearings in the longitudinal direction restrict the pier more strongly and the ratio of longitudinal natural frequencies increases gradually. When the pier height is 23 m, the frequency ratio is 2 times of 9 m.

In actual earthquakes, there is a time difference between horizontal and vertical earthquakes. At the same time, there may be several vertical separations under earthquake action, resulting in the time of vertical separation being uncertain. The dynamic deformation of separated pier is affected by displacement, velocity, and forced vibration after separation. Compared with the unseparated state, the initial velocity of separation and the displacement response amplitude caused by forced vibration are affected by the structural frequency. The longitudinal natural frequency of the separated pier is lower, resulting in a larger deformation amplitude. Considering the phase angle difference, the change of the longitudinal deformation of the bridge pier after separation is given in equation (15). The extreme value of the longitudinal deformation of the bridge pier after separation is the maximum value of the sum of the first two terms, superimposed on the maximum value of the third term.

$$\begin{aligned}\overline{W}_d(x,t) = &\left[\sum_{n=1}^{5}\overline{\varphi}_{nr}(\xi)\omega_{nr}(t_1) + \sum_{n=1}^{5}\frac{\overline{A}_{rn}\overline{B}_{rn}\omega_0^2 B_0}{\left(\omega_0^2-\omega_{nr}^2\right)}\sin\ \omega_0 t_1\right]\cos\ \omega_{nr}(t-t_1)\\ &+\frac{\left[\sum_{n=1}^{5}\overline{\varphi}_{nr}(\xi)\dot{\omega}_{nr}(t_1) + \sum_{n=1}^{5}\left(\overline{A}_{rn}\overline{B}_{rn}\omega_0^2 B_0/\omega_{nr}\left(\omega_0^2-\omega_{nr}^2\right)\right)\omega_0\cos\ \omega_0 t_1\right]}{\omega_{nr}}\sin\ \omega_{nr}(t-t_1)\\ &-\sum_{n=1}^{5}\frac{\overline{A}_{rn}\overline{B}_{rn}\omega_0^2 B_0}{\omega_{nr}\left(\omega_0^2-\omega_{nr}^2\right)}\omega_{nr}\sin\ \omega_0 t.\end{aligned} \tag{15}$$

Figure 6shows the maximum longitudinal deformation of pier top at different heights. When there is no vertical separation of the pier-beam, the deformation of pier top reaches the maximum value when $\omega_0 = \omega_1$, and when the seismic excitation frequency is close to the first-order longitudinal natural vibration frequency of the bridge, it decreases monotonically. When the vertical seismic excitation causes the separation between the main beam and the pier (for the low pier) because the longitudinal natural frequency changes very little before and after separation, the change trend is consistent with that of the unseparated state, and the separation has little influence on the deformation of the pier top. With the increase of pier height, pier-beam separation increases the longitudinal dynamic response of pier top.

Table 2 shows the longitudinal natural frequency ratios of pier beams before and after separation under different

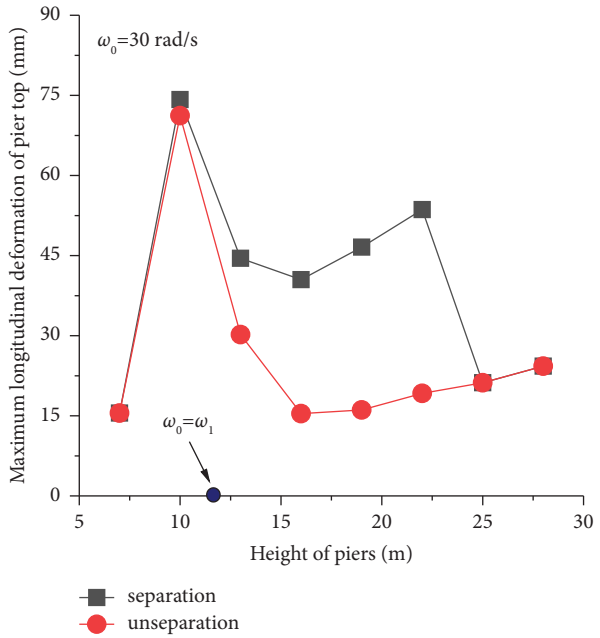

Figure 6: Deformation of pier top at different heights.

Table 1: The Ratio of longitudinal frequencies before and after pier separation at different heights.

Height of piers/m	Ratio of longitudinal natural frequencies ω_1/ω_{1r}
7	1.01
10	1.05
13	1.14
16	1.32
19	1.57
22	1.84
25	2.09
28	2.28

pier diameters. With the increase of pier diameter, the ratio of longitudinal frequencies before and after separation gradually decreases, and when the pier diameter exceeds 1.7 m, the longitudinal frequencies before and after separation almost remain unchanged.

Figure 7 shows the longitudinal deformation at the top of the pier at different diameters. With the increase of pier diameter, the excitation frequency is close to the first-order natural frequency, and the maximum value of longitudinal deformation at the top of the pier increases monotonically. However, the longitudinal natural vibration frequency decreases gradually and approaches 1 before and after pier-beam separation. When vertical separation of the pier-beam is considered, the longitudinal deformation at the top of pier increases greatly, and when a peak value is reached, the longitudinal deformation at the top of the pier decreases greatly, because the ratio of longitudinal vibration frequency decreases gradually before and after separation, and the influence of separation on the pier deformation decreases gradually.

It should be noted that the cross-sectional shape of piers in engineering construction is not only circular but also

Table 2: Longitudinal frequency ratios of piers with different diameters before and after separation.

Diameter of the piers D/m	Ratio of longitudinal natural frequencies ω_1/ω_{1r}
1.0	1.91
1.1	1.69
1.2	1.49
1.3	1.35
1.4	1.23
1.5	1.16
1.6	1.11
1.7	1.08

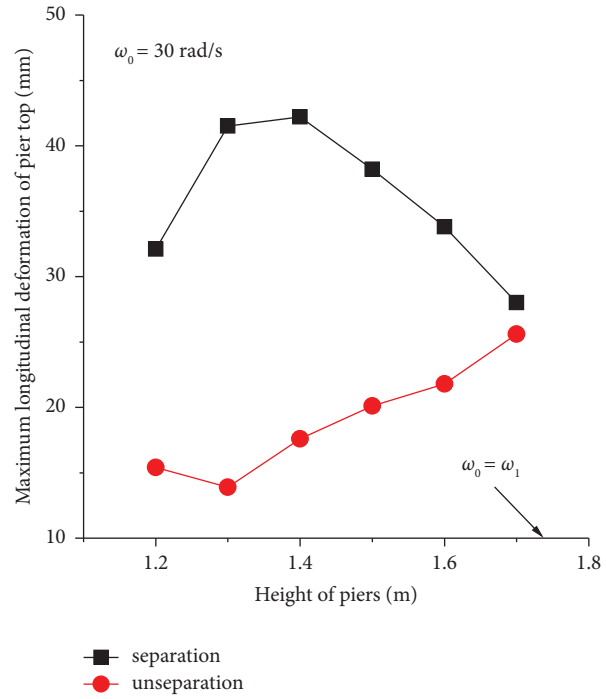

Figure 7: Deformation of pier top at different diameters.

rectangular. Through the previous analysis, it is pointed out that the change of the longitudinal deformation of the pier after the separation of the pier-beam is caused by the change of the natural frequency of the pier. The smaller the flexural stiffness of the pier, the greater the longitudinal change of the pier top before and after separation. Therefore, when the cross-sectional area of the pier is smaller and the aspect ratio is larger, the vertical separation has a greater impact on the longitudinal dynamic response of the pier.

5. The Pier Failure Mode

The actual eccentric collision diagram of the bridge is shown in Figure 8(a). The pier deforms in the horizontal direction under seismic excitation. The collision eccentricity is different at different heights of piers. For rubber bearing bridge, the pier failure is concentrated at the bottom of the pier. To simplify the calculation, the equivalent simplified model of Figure 8(b) was used.

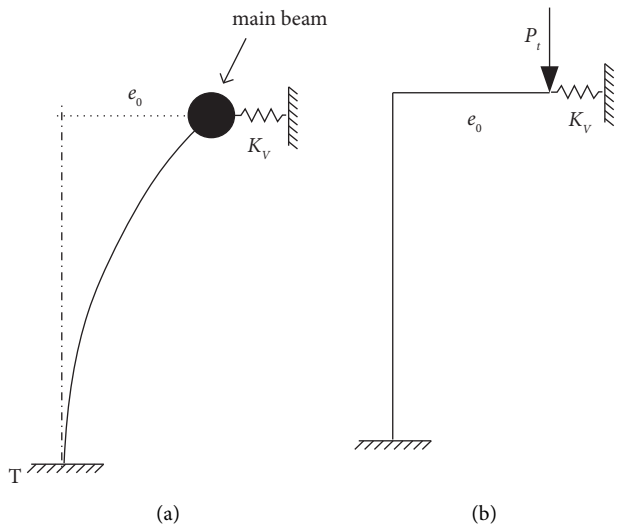

FIGURE 8: The calculation model of eccentric collision: (a) the collision model; (b) the simplified model.

5.1. Compression Damage. With the increase of pier diameter, the design value of normal section compressive capacity of pier increases monotonically. For pier compression failure, the pier height is selected to carry out the analysis. The maximum separation pressure at the bottom of the pier is shown in Figure 9. When the vertical separation of the pier and beam occurs, with the increase of pier height, the maximum value and allowable value of the pressure at the bottom of the pier decrease monotonously, as a result the pier has the risk of compression failure. However, when the pier beam does not separate, the longitudinal deformation of the pier decreases significantly, the allowable pressure of the pier increases significantly, and the pier is in the safe range.

5.2. Bending Damage. For girder bridges with plate-type rubber bearings, the bending failure of pier mainly occurs at the bottom of pier. The bending moment at the bottom of the pier is mainly composed of following three parts: the bending moment M_Z caused by longitudinal forced vibration, the bending moment M_C caused by eccentric collision, and the bending moment M_V caused by bearing shear. To simplify the calculation, the calculation formula of each bending moment is as follows:

$$\begin{cases} M_C = F_{\max} \times \eta \times \Delta\, d, \\ M_Z = \dfrac{E_r I_r \partial^2 U_d}{\partial \xi^2}, \\ M_V = K_V \times \eta \times \Delta\, d \times H. \end{cases} \tag{16}$$

Eccentricity of circular section reinforced concrete with longitudinal reinforcement uniformly distributed along the periphery can refer to code [26]. See the following formula for details:

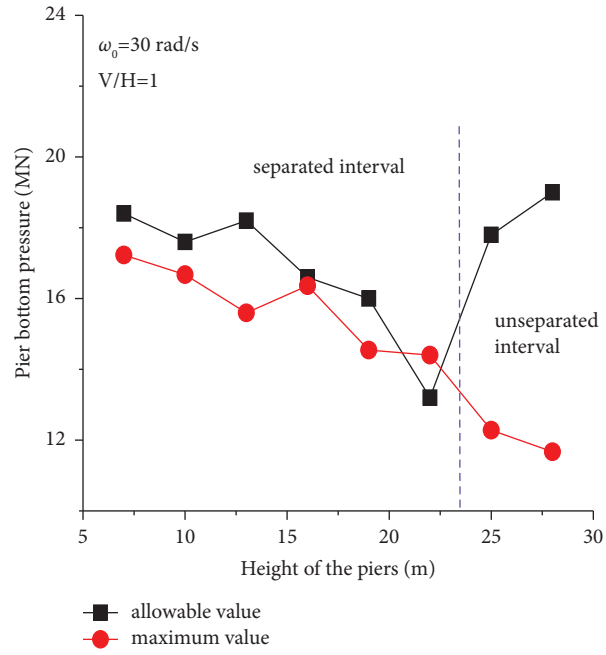

FIGURE 9: Compression of piers under different heights.

$$N = \alpha f_{cd} A_r \left(1 - \frac{\sin 2\,\pi\alpha}{2\pi\alpha}\right) + (\alpha - \alpha_t) f_{sd} A_s,$$
$$M_{ud} = \frac{2}{3} f_{cd} A_r \frac{\sin^3 \pi\alpha}{\pi} + f_{sd} A_s r_s \frac{\sin \pi\alpha + \sin \pi\alpha_t}{\pi}. \tag{17}$$

Figure 10 shows the variation of bending moments at the bottom of pier with pier height under seismic excitation. With the increase of the pier height, the longitudinal dynamic response of the pier will be affected by the separation $\omega_1 = \omega_0$. It reaches the extreme value. When the pier height is more than 10 m and the structure is separated, the bending moment at the bottom of the pier by the shear force basically reaches the limit state due to the limited shear deformation of the rubber bearing. The bending moment at the bottom of pier caused by eccentric compression is $\omega_1 = \omega_0$. At this time, the seismic characteristic frequency is close to the longitudinal natural frequency of the bridge, and the pier top has a large deformation. With the increase of pier height, the vertical contact force of pier beam decreases gradually, but the deformation of pier top caused by separation continues to increase, and the deformation caused by eccentric pressure first decreases and then increases slowly.

Figure 11 shows the bending failure of piers with different heights under earthquake excitation. ω_1 is near ω_0. At this time, the seismic characteristic frequency is close to the vertical and longitudinal natural frequencies of the bridge and the bending moment at the bottom of the pier. With the increase of pier height, the total bending moment at the bottom of pier decreases gradually and fluctuates slightly near the allowable bending moment. When the pier height $H > 23$ m, the pier beam does not have vertical separation, the longitudinal dynamic response is greatly reduced, and the pier will not be subjected to bending failure.

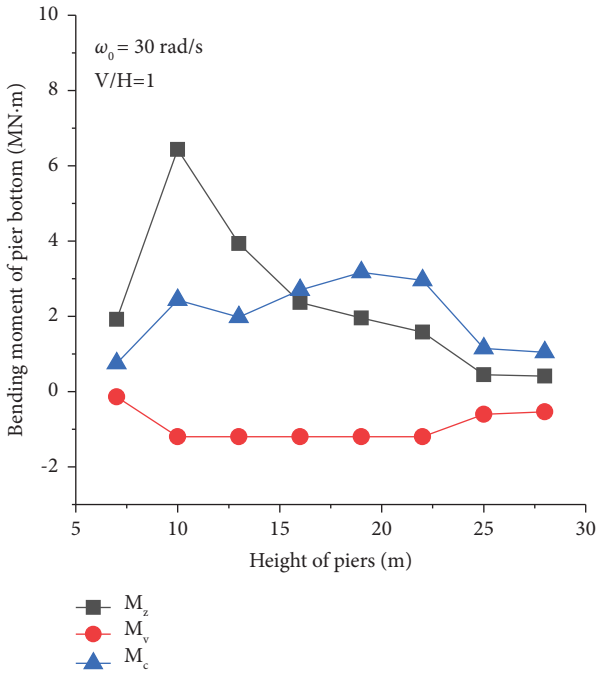

Figure 10: Bending moment at the bottom of pier under different pier heights.

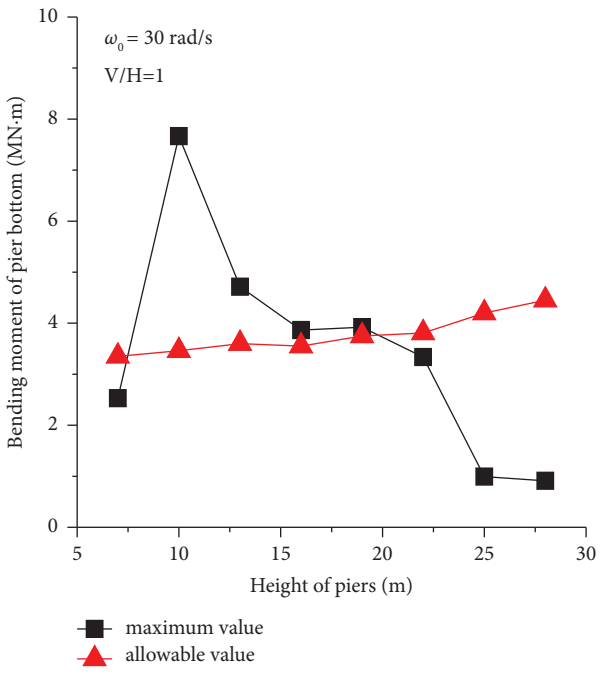

Figure 11: Bending of pier bottom under different pier heights.

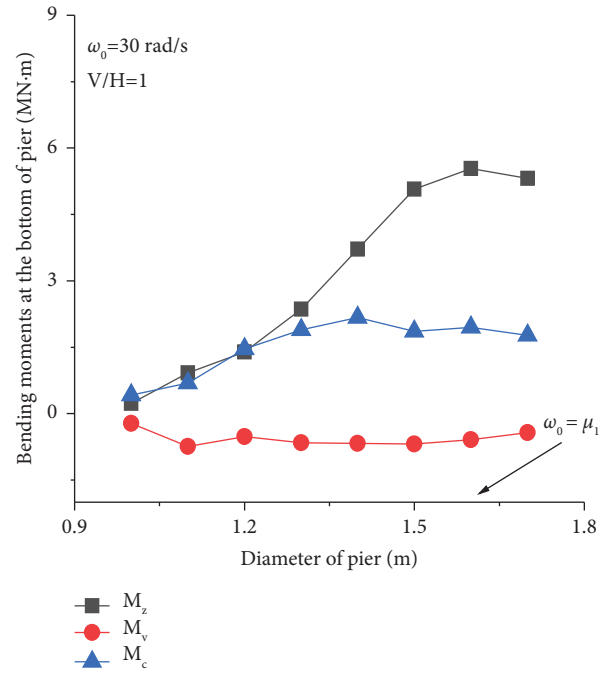

Figure 12: Bending moments at the bottom of piers with different diameters.

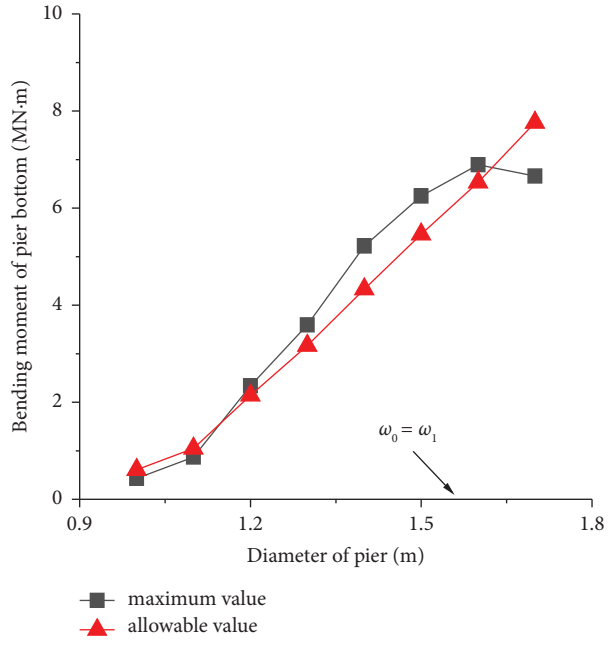

Figure 13: Bending at the bottom of the pier with different diameters.

Figure 12 shows bending moments at the bottom of pier under different pier diameters. The pier and beam separation increased the longitudinal deformation at the top of the pier, and the bending moment of each part increased significantly. With the increase of the pier area, the longitudinal deformation at the top of the pier increases first and then decreases. The bending moment generated by eccentric collision and rubber bearing shear increases first and then decreases, while the bending moment generated by forced vibration increases gradually due to the influence of inertia force.

Figure 13 shows the bending failure of pier bottom under different pier diameters under earthquake excitation. With the increase of pier diameter, the total bending moment and

allowable bending moment increase monotonically. When the diameter is more than 1.7 m, the longitudinal natural vibration frequency of the bridge is gradually away from the seismic characteristic frequency, the dynamic response of separation to the pier decreases, and the pier is gradually in the safe zone.

5.3. Shear Damage. In plate rubber bearing bridge, the shear failure of the pier is concentrated at the bottom of the pier. In addition to the structural size and reinforcement, the shear failure of the pier bottom is affected by the change of the pier bottom pressure and bending moment. The previous analysis indicates that the increase of the pier pressure and longitudinal deformation caused by the vertical separation of the pier-beam will increase the bending moment at the bottom of the pier and lead to the shear failure of the concrete pier. Code [26] gives the shear calculation formula of the pier, and the shear strength of inclined section along the horizontal direction of pier column plastic hinge interval is calculated according to equations (18) and (19).

$$V_c \le \phi (V_c + V_s),$$
$$V_c = 0.1 v_c A_e, \tag{18}$$

$$v_c = \begin{cases} 0, & P_c \le 0, \\ \lambda\left(1 + \dfrac{P_c}{1.38 A_g}\right)\sqrt{f_{cd}} \le \min \begin{cases} 0.355\sqrt{f_{cd}} \\ 1.47\lambda\sqrt{f_{cd}} \end{cases}, & P_c > 0. \end{cases} \tag{19}$$

The bottom of the pier is damaged by seismic excitation. Compared with Figure 14 the overall change trend of shear is similar to that of bending, but it is somewhat different from the failure zone under bending. For the pier with lower height, shear failure occurs instead of bending failure. When the pier height $H > 17$ m, the allowable shear force of the pier is greater than the total shear force at the bottom; there is no shear failure of the pier. When the vertical seismic excitation frequency is close to the vertical natural frequency of the bridge, for the pier with lower height, the shear failure occurs at the bottom of the pier, and with the increase of the height, the bending moment failure occurs gradually.

Figure 15shows the bottom failure of different pier diameters under seismic excitation. When the pier area is low, there is the failure of the pier under pressure. With the increase of pier diameter, the increased pier stiffness increases the vertical impact force of the pier-beam, but the increase is less than the pressure required for strength failure and stability failure, and the allowable pressure for stability failure increases more than the allowable pressure for strength failure. With the increase of pier section area, the risk of pier compression and instability is gradually reduced.

5.4. Change of Failure Modes of Bridge Piers at Different Heights. Through the above analysis, it can be found that

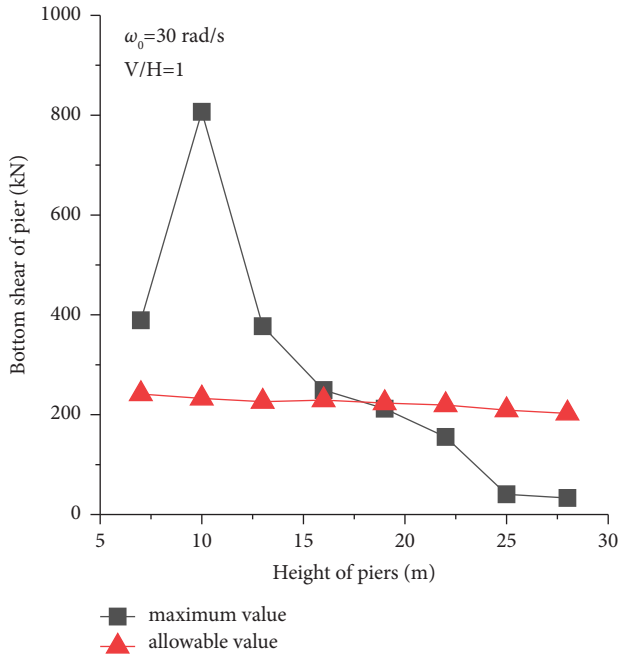

Figure 14: Shear condition of the pier bottom under different pier heights.

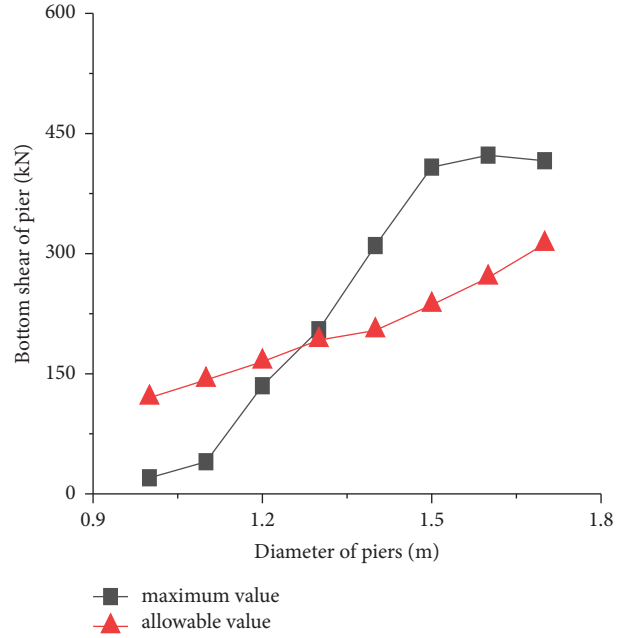

Figure 15: Shear conditions at the bottom of the pier with different diameters.

there are many failure modes of piers with different heights in the separation zone of the pier and beam. In order to study the influence of different pier height on structural failure, the critical value of longitudinal deformation at the top of the pier is used to judge whether the structure is in the safe range. The results show that the vertical contact force of the pier-beam of different height piers is concentrated in 2 $F_c \sim 4F_c$. In order to facilitate the study, the vertical contact

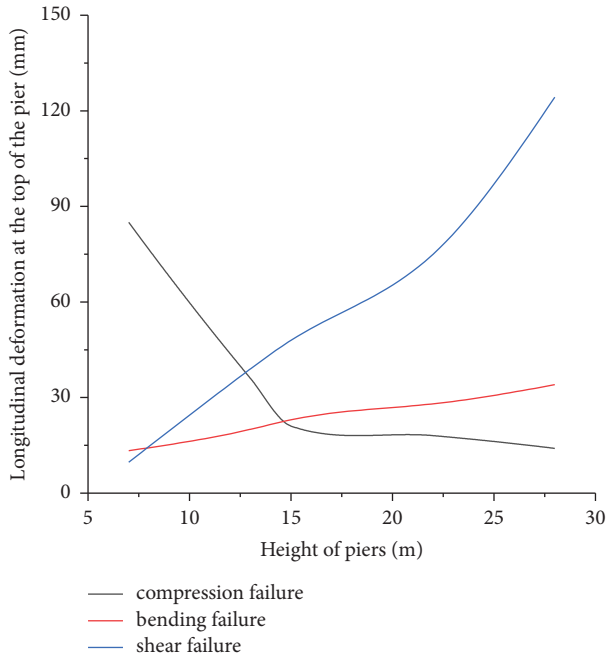

Figure 16: Failure modes of piers with different pier heights.

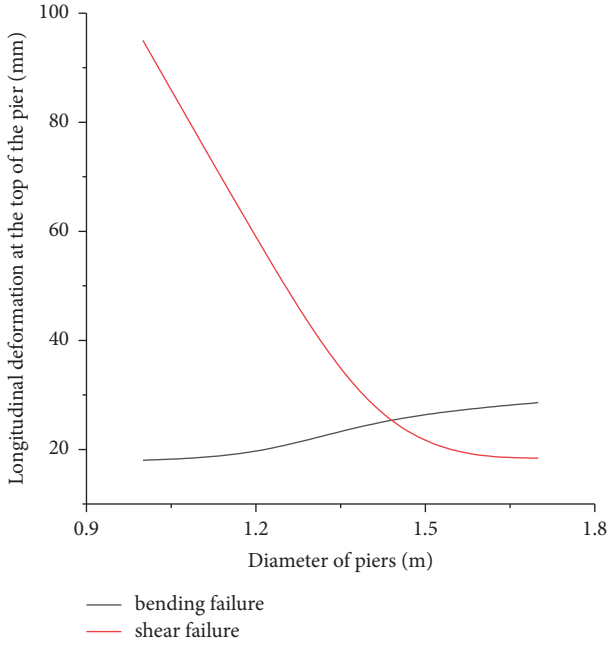

Figure 17: Failure modes of the pier under different pier areas.

force of the pier-beam is $3F_c$. The failure modes of bridge piers under different pier heights are analyzed.

Figure 16 shows the failure mode diagram of the pier at different pier heights. When the pier height is lower, the pier height will increase first. When $H > 14.5$ m, the pier will be damaged by compression. With the increase of the pier height, the longitudinal restraint of rubber bearing on the pier increases. When $H > 20$ m, the effective height of the pier increases slowly and the influence of pier height on pier instability is small.

The change of pier area significantly changes pier strength and stable admissible bearing capacity. Figure 17 shows the pier failure conditions under different pier areas. As the area change significantly affects the compression and stability failure, only the bending and shear failure at the bottom of the pier are considered here. Considering that the change of pier cross section diameter significantly affects the compressive capacity of the pier, the vertical contact force of the pier-beam is $2F_c$. When the pier area is small, bending failure occurs, and with the increase of diameter, the pier gradually becomes shear failure.

6. Conclusion

This study considers the effect of different pier sizes on pier failure under seismic excitation. The influence of structural parameters on vertical separation of the pier-beam, the vertical impact force of the pier-beam, and the maximum value of longitudinal displacement of the pier top were determined by calculating the dynamic response of the bridge. The influence of bridge structural parameters on pier failure modes is proposed by comparing the calculated results with the code. The following conclusions are obtained from the analysis:

(1) The higher the pier height, the smaller the section size is, the larger the vertical seismic acceleration required to separate the pier beam is, the smaller the vertical contact force of the pier beam is, and the greater the most adverse value of the longitudinal deformation of the pier caused by separation is.

(2) Separation will increase the risk of pier failure, and with the increase of pier height, the first failure mode is shear failure, bending failure, and compression failure.

(3) Considering pier and beam separation, with the increase of pier diameter, the primary failure mode of pier changes from bending failure to shear failure.

Data Availability

The original data can be obtained by contacting the corresponding authors.

Conflicts of Interest

The authors declare that they have no conflicts of interest.

Acknowledgments

This study was supported by Science and Technology Project of Jiangxi Education Department: GJJ202915.

References

[1] S. Thapa, Y. Shrestha, and D. Gautam, "Seismic fragility analysis of RC bridges in high seismic regions under horizontal and simultaneous horizontal and vertical excitations," *Structures*, vol. 37, no. 3, pp. 284–294, 2022.

[2] Y. H. Shao, Y. Y. Wei, T. Yang, M. Ni, and J. Zhong, "Empirical models of bridge seismic fragility surface considering the vertical effect of near-fault ground motions," *Structures*, vol. 34, pp. 2962–2973, 2021.

[3] H. N. Li, S. Y. Xiao, and L. S. Huo, "Damage investigation and analysis of Engineering structures in the Wenchuan earthquake," *Journal of Building Structures*, vol. 29, pp. 10–19, 2008.

[4] W. L. Zhuang, Z. Y. Liu, and J. S. Jiang, "Earthquake-induced damage analysis of highway bridges in Wenchuan earthquake and countermeasures," *Chinese Journal of Rock Mechanics and Engineering*, vol. 28, pp. 1377–1387, 2009.

[5] A. J. Papazoglou and A. S. Elnashai, "Analytical and field evidence of the damaging effect of vertical earthquake ground motion," *Earthquake Engineering & Structural Dynamics*, vol. 25, no. 10, pp. 1109–1137, 1996.

[6] H. Y. Wang and L. L. Xie, "Characteristics of near-fault strong ground motions," *Journal of Harbin Institute of Technology*, vol. 38, no. 12, pp. 2070–2076, 2006.

[7] N. N. Ambraseys and J. Douglas, "Near-field horizontal and vertical earthquake ground motions," *Soil Dynamics and Earthquake Engineering*, vol. 23, no. 1, pp. 1–18, 2003.

[8] R. K. McGuire, W. J. Silva, and R. Kenneally, "New seismic design spectra for nuclear power plants," *Nuclear Engineering and Design*, vol. 203, no. 2-3, pp. 249–257, 2001.

[9] W. Silva, *Characteristics of Vertical Ground Motions for Applications to Engineering Design*, National Center for Earthquake Engineering Research, New York, NY, USA, 1997.

[10] N. Abrahamson and J. Litehiser, "Attenuation of vertical peak acceleration," *Bulletin of the Seismological Society of America*, vol. 79, no. 3, pp. 549–580, 1989.

[11] S. W. Geng and X. X. Tao, "The ratios of vertical to horizontal acceleration response spectra," *Earthquake Engineering and Engineering Vibration*, vol. 24, no. 5, pp. 33–38, 2005.

[12] Z. H. Zhou, Y. N. Zhou, and T. Lu, "Study on characteristics of vertical ground motion," *Earthquake Engineering and Engineering Vibration*, vol. 23, no. 3, pp. 25–29, 2003.

[13] A. Elgamal and L. C. He, "Vertical earthquake ground motion records: an overview," *Journal of Earthquake Engineering*, vol. 8, no. 5, pp. 663–697, 2004.

[14] Y. Bozorgnia and M. Niazi, "Distance scaling of vertical and horizontal response spectra of the Loma Prieta earthquake," *Earthquake Engineering & Structural Dynamics*, vol. 22, no. 8, pp. 695–707, 1993.

[15] P. Liu, Q. F. Luo, and X. Z. Chen, "Vertical ground motion attenuation relationship of Wenchuan earthquake," *Journal of Harbin Institute of Technology*, vol. 52, no. 2, pp. 119–128, 2020.

[16] J. H. Wang, M. W. Huang, K. C. Chen, R. Hwang, and W. Chang, "Aspects of characteristics of near fault ground motions of the 1999 chi chi (Taiwan) earthquake," *Journal of the Chinese Institute of Engineers*, vol. 25, no. 5, pp. 507–519, 2002.

[17] S. Tanimura, K. Mimura, T. Nonaka, and W. Zhu, "Dynamic failure of structures due to the great Hanshin-Awaji earthquake," *International Journal of Impact Engineering*, vol. 24, no. 6-7, pp. 583–596, 2000.

[18] M. F. Li and Y. F. Xu, "Seismic response and performance evaluation of asymmetric continuous beam bridge in meizoseismal areas," *Chin Earthquake Engineering Journal*, vol. 42, no. 5, pp. 1276–1282, 2020.

[19] Y. Zuo, G. J. Sun, and H. J. Li, "Comparison and research of unseating prevention measures in seismic codes of China and foreign countries," *Journal of Disaster Prevention and Mitigation Engineering*, vol. 36, pp. 617–623, 2016.

[20] D. Wang and L. L. Xie, "Attenuation of peak ground accelerations from the great Wenchuan earthquake," *Earthquake Engineering and Engineering Vibration*, vol. 8, no. 2, pp. 179–188, 2009.

[21] D. Lavallee and R. J. Archuleta, "Stochastic modeling of slip spatial complexities for the 1979 Imperial Valley, California, earthquake," *Geophysical Research Letters*, vol. 30, no. 5, pp. 50–54, 2003.

[22] Y. Fukushima, Irikura, and T. Uetake, "Characteristics of observed peak amplitude for strong ground motion from the 1995 hyogoken nanbu (kobe) earthquake," *Bulletin of the Seismological Society of America*, vol. 90, no. 3, pp. 545–565, 2000.

[23] S. Tanimura, T. Sato, T. Umeda, K. Mimura, and O Yoshikawa, "A note on dynamic fracture of the bridge bearing due to the great Hanshin–Awaji earthquake," *International Journal of Impact Engineering*, vol. 27, no. 2, pp. 153–160, 2002.

[24] H. Yang and X. Yin, "Transient responses of girder bridges with vertical poundings under near-fault vertical earthquake," *Earthquake Engineering & Structural Dynamics*, vol. 44, no. 15, pp. 2637–2657, 2015.

[25] S. Chen, H. Xia, and W. An, "Theoretical Investigation on Multiple Separation of Bridge under Near-Fault Vertical Ground Motion," *Mathematical Problems in Engineering*, vol. 2021, Article ID 6634917, 9 pages, 2021.

[26] Cjj 166-2011, *Code for Seismic Design of Urban Bridges*, Ministry of Housing and Urban-Rural Development of the People's Republic of China, Beijing, China, 2011.